# TOI-1408: Discovery and Photodynamical Modeling of a Small Inner Companion to a Hot Jupiter Revealed by Transit Timing Variations

Judith Korth, Priyanka Chaturvedi, Hannu Parviainen, Ilaria Carleo, Michael Endl, Eike W. Guenther, Grzegorz Nowak, Carina M. Persson, Phillip J. Macqueen, Alexander J. Mustill, et al.

▶ **To cite this version:**

Judith Korth, Priyanka Chaturvedi, Hannu Parviainen, Ilaria Carleo, Michael Endl, et al.. TOI-1408: Discovery and Photodynamical Modeling of a Small Inner Companion to a Hot Jupiter Revealed by Transit Timing Variations. The Astrophysical Journal Letters, 2024, 971, 10.3847/2041-8213/ad65fd . insu-04726431

**HAL Id: insu-04726431**

**https://insu.hal.science/insu-04726431v1**

Submitted on 9 Oct 2024

**HAL** is a multi-disciplinary open access archive for the deposit and dissemination of scientific research documents, whether they are published or not. The documents may come from teaching and research institutions in France or abroad, or from public or private research centers.

L'archive ouverte pluridisciplinaire **HAL**, est destinée au dépôt et à la diffusion de documents scientifiques de niveau recherche, publiés ou non, émanant des établissements d'enseignement et de recherche français ou étrangers, des laboratoires publics ou privés.

Distributed under a Creative Commons Attribution 4.0 International License

The Astrophysical Journal Letters, 971:L28 (14pp), 2024 August 20 https://doi.org/10.3847/2041-8213/ad65fd
© 2024. The Author(s). Published by the American Astronomical Society.
OPEN ACCESS

# TOI-1408: Discovery and Photodynamical Modeling of a Small Inner Companion to a Hot Jupiter Revealed by Transit Timing Variations

Judith Korth[1], Priyanka Chaturvedi[2,3], Hannu Parviainen[4,5], Ilaria Carleo[6,5,4], Michael Endl[7,8], Eike W. Guenther[2], Grzegorz Nowak[9,5,4], Carina M. Persson[10], Phillip J. MacQueen[7], Alexander J. Mustill[1], Juan Cabrera[11], William D. Cochran[7,8], Jorge Lillo-Box[12], David Hobbs[1], Felipe Murgas[5,4], Michael Greklek-McKeon[13], Hanna Kellermann[14], Guillaume Hébrard[15,16], Akihiko Fukui[17,5], Enric Pallé[5,4], Jon M. Jenkins[18], Joseph D. Twicken[19,18], Karen A. Collins[20], Samuel N. Quinn[20], Ján Šubjak[21,20], Paul G. Beck[4,5], Davide Gandolfi[22], Savita Mathur[5,4], Hans J. Deeg[5,4], David W. Latham[20], Simon Albrecht[23], David Barrado[12], Isabelle Boisse[16,24], Hervé Bouy[25,26], Xavier Delfosse[27], Olivier Demangeon[28], Rafael A. García[29], Artie P. Hatzes[2], Neda Heidari[15], Kai Ikuta[30], Petr Kabáth[21], Heather A. Knutson[13], John Livingston[31,32,33], Eder Martioli[34,15], María Morales-Calderón[12], Giuseppe Morello[35,5], Norio Narita[17,31,5], Jaume Orell-Miquel[5,4], Hanna L. M. Osborne[36,37], Dinil B. Palakkatharappil[29], Viktoria Pinter[38,39], Seth Redfield[40], Howard M. Relles[20], Richard P. Schwarz[20], Sara Seager[41,42,43], Avi Shporer[41], Marek Skarka[21,44], Gregor Srdoc[45], Monika Stangret[46], Luis Thomas[14,47], Vincent Van Eylen[36], Noriharu Watanabe[30], and Joshua N. Winn[48]

[1] Lund Observatory, Division of Astrophysics, Department of Physics, Lund University, Box 118, 22100 Lund, Sweden; judithkorth@googlemail.com
[2] Thüringer Landessternwarte Tautenburg, Sternwarte 5, 07778 Tautenburg, Germany
[3] Tata Institute of Fundamental Research (TIFR), Homi Bhabha Road, Colaba, Mumbai - 400005, India
[4] Departamento de Astrofísica, Universidad de La Laguna (ULL), E-38206 La Laguna, Tenerife, Spain
[5] Instituto de Astrofísica de Canarias (IAC), E-38205 La Laguna, Tenerife, Spain
[6] INAF—Osservatorio Astrofisico di Torino, Via Osservatorio 20, I-10025, Pino Torinese, Italy
[7] McDonald Observatory, The University of Texas, Austin TX, USA
[8] Center for Planetary Systems Habitability, The University of Texas, Austin TX, USA
[9] Institute of Astronomy, Faculty of Physics, Astronomy and Informatics, Nicolaus Copernicus University, Grudziądzka 5, 87-100 Toruń, Poland
[10] Department of Space, Earth and Environment, Chalmers University of Technology, Onsala Space Observatory, SE-439 92 Onsala, Sweden
[11] Institut für Planetenforschung, Deutsches Zentrum für Luft- und Raumfahrt, Rutherfordstr. 2, 12489 Berlin, Germany
[12] Centro de Astrobiologiía (CAB), CSIC-INTA, Camino Bajo del Castillo s/n, ESAC campus, 28692, Villanueva de la Cañada, Madrid, Spain
[13] Division of Geological and Planetary Sciences, California Institute of Technology, Pasadena, CA, 91125, USA
[14] University Observatory Munich, Faculty of Physics, Ludwig-Maximilians-Universität München, Scheinerstr. 1, 81679 Munich, Germany
[15] Institut d'astrophysique de Paris, UMR7095 CNRS, Université Pierre & Marie Curie, 98bis boulevard Arago, 75014 Paris, France
[16] Observatoire de Haute-Provence, CNRS, Université d'Aix-Marseille, 04870 Saint-Michel-l'Observatoire, France
[17] Komaba Institute for Science, The University of Tokyo, 3-8-1 Komaba, Meguro, Tokyo 153-8902, Japan
[18] NASA Ames Research Center, Moffett Field, CA 94035, USA
[19] SETI Institute, Mountain View, CA 94043, USA
[20] Center for Astrophysics |Harvard & Smithsonian, 60 Garden Street, Cambridge, MA 02138, USA
[21] Astronomical Institute, Czech Academy of Sciences, Fričova 298, 251 65, Ondřejov, Czech Republic
[22] Dipartimento di Fisica, Università degli Studi di Torino, via Pietro Giuria 1, I-10125, Torino, Italy
[23] Stellar Astrophysics Centre, Department of Physics and Astronomy, Aarhus University, Ny Munkegade 120, DK-8000 Aarhus C, Denmark
[24] Aix Marseille Univ, CNRS, CNES, LAM, Marseille, France
[25] Laboratoire d'astrophysique de Bordeaux, Univ. Bordeaux, CNRS, B18N, allée Geoffroy Saint-Hilaire, 33615 Pessac, France
[26] Institut universitaire de France (IUF), 1 rue Descartes, 75231 Paris CEDEX 05, France
[27] Université Grenoble Alpes, CNRS, IPAG, 38000 Grenoble, France
[28] Instituto de Astrofísica e Ciências do Espaço, Universidade do Porto, CAUP, Rua das Estrelas, 4150-762 Porto, Portugal
[29] Université Paris-Saclay, Université Paris Cité, CEA, CNRS, AIM, 91191, Gif-sur-Yvette, France
[30] Department of Multi-Disciplinary Sciences, Graduate School of Arts and Sciences, The University of Tokyo, 3-8-1 Komaba, Meguro, Tokyo 153-8902, Japan
[31] Astrobiology Center, 2-21-1 Osawa, Mitaka, Tokyo 181-8588, Japan
[32] National Astronomical Observatory of Japan, 2-21-1 Osawa, Mitaka, Tokyo 181-8588, Japan
[33] Astronomical Science Program, Graduate University for Advanced Studies, SOKENDAI, 2-21-1, Osawa, Mitaka, Tokyo, 181-8588, Japan
[34] Laboratório Nacional de Astrofísica, Rua Estados Unidos 154, 1006 37504-364, Itajubá - MG, Brazil
[35] Instituto de Astrofísica de Andalucía (IAA-CSIC), Gta. de la Astronomía s/n, 18008 Granada, Granada, Spain
[36] Mullard Space Science Laboratory, University College London, Holmbury St Mary, Dorking, Surrey RH5 6NT, UK
[37] European Southern Observatory, Karl-Schwarzschild-Strae 2, Garching bei München D-85748, Germany
[38] Nordic Optical Telescope, Rambla José Ana Fernandez Pérez 7, 38711, Breña Baja, Spain
[39] University of Craiova, Alexandru Ioan Cuza 13, 200585, Craiova, Romania
[40] Astronomy Department and Van Vleck Observatory, Wesleyan University, Middletown, CT 06459, USA
[41] Department of Physics and Kavli Institute for Astrophysics and Space Research, Massachusetts Institute of Technology, Cambridge, MA 02139, USA
[42] Department of Earth, Atmospheric and Planetary Sciences, Massachusetts Institute of Technology, Cambridge, MA 02139, USA
[43] Department of Aeronautics and Astronautics, MIT, 77 Massachusetts Avenue, Cambridge, MA 02139, USA
[44] Department of Theoretical Physics and Astrophysics, Faculty of Science, Masaryk University, Kotlářská 267/2, 611 37 Brno, Czech Republic
[45] Kotizarovci Observatory, Sarsoni 90, 51216 Viskovo, Croatia
[46] INAF — Osservatorio Astronomico di Padova, Vicolo dell'Osservatorio 5, 35122, Padova, Italy
[47] Max-Planck Institute for Extraterrestrial Physics, Giessenbachstrasse 1, D-85748 Garching, Germany

[48] Department of Astrophysical Sciences, Princeton University, Princeton, NJ 08544, USA
*Received 2024 June 25; accepted 2024 July 12; published 2024 August 12*


## Abstract

We report the discovery and characterization of a small planet, TOI-1408 c, on a 2.2 day orbit located interior to a previously known hot Jupiter, TOI-1408 b ($P = 4.42$ days, $M = 1.86 \pm 0.02\,M_{\rm Jup}$, $R = 2.4 \pm 0.5\,R_{\rm Jup}$) that exhibits grazing transits. The two planets are near 2:1 period commensurability, resulting in significant transit timing variations (TTVs) for both planets and transit duration variations for the inner planet. The TTV amplitude for TOI-1408 c is 15% of the planet's orbital period, marking the largest TTV amplitude relative to the orbital period measured to date. Photodynamical modeling of ground-based radial velocity (RV) observations and transit light curves obtained with the Transiting Exoplanet Survey Satellite and ground-based facilities leads to an inner planet radius of $2.22 \pm 0.06\,R_{\oplus}$ and mass of $7.6 \pm 0.2\,M_{\oplus}$ that locates the planet into the sub-Neptune regime. The proximity to the 2:1 period commensurability leads to the libration of the resonant argument of the inner planet. The RV measurements support the existence of a third body with an orbital period of several thousand days. This discovery places the system among the rare systems featuring a hot Jupiter accompanied by an inner low-mass planet.


*Unified Astronomy Thesaurus concepts:* Exoplanet dynamics (490); Hot Jupiters (753); Hot Neptunes (754); Transit timing variation method (1710); Transit photometry (1709); Radial velocity (1332)

*Materials only available in the online version of record: machine-readable tables*

## 1. Introduction

The discovery of the first exoplanet around a main-sequence star, 51 Peg b, significantly advanced our understanding of planetary systems due to its dissimilarity (e.g., short orbital period) from any known planets in our solar system (Mayor & Queloz 1995). Nearly 30 yr later, the origins of such hot Jupiters (HJs)—gas giants with orbital periods less than 10 days and with planet masses higher than 0.1 $M_{\rm Jup}$ following the definition from Wang et al. (2015)—remain elusive. Theories suggest that HJs could form in situ (e.g., Batygin et al. 2016), migrate inward from beyond the ice line through the interaction with the gas disk during formation (e.g., Lin et al. 1996), or undergo high-eccentricity migration (HEM; Rasio & Ford 1996) at a later stage. For an overview, see Dawson & Johnson (2018) and references therein.

The lack of detections of low-mass planets interior to HJs (Steffen et al. 2012; Mustill et al. 2015; Huang et al. 2016; Hord et al. 2021) is a key argument supporting HEM as the dominant formation channel. However, exceptional systems where an inner low-mass planet accompanies an HJ have been detected, such as WASP-47 (Hellier et al. 2012; Becker et al. 2015; Nascimbeni et al. 2023), WASP-84 (Anderson et al. 2014; Maciejewski et al. 2023), Kepler-730 (Zhu et al. 2018; Cañas et al. 2019), TOI-2000 (Sha et al. 2023), WASP-132 (Hellier et al. 2017; Hord et al. 2022; Grieves et al. 2024), and TOI-1130 (Huang et al. 2020a; Korth et al. 2023). These systems cannot be explained by HEM and require a dynamically quiet formation process, such as disk migration (Fogg & Nelson 2005, 2007; Wu & He 2023; Wu et al. 2023; He et al. 2024), or a less quiet process, such as in situ formation (Poon et al. 2021).

In this Letter, we present the discovery of another of these rare systems containing an HJ and a low-mass planet close to the 2:1 period commensurability, resulting in measurable transit timing variations (TTVs), similar to TOI-1130. We report the discovery and characterization of a small planet, TOI-1408 c, interior to a known grazing hot Jupiter, TOI-1408 b, discovered using Transiting Exoplanet Survey Satellite (TESS; Ricker et al. 2015) photometry and confirmed by Galazutdinov et al. (2023). Our analysis also refines the orbital and geometric properties of TOI-1408 b.

Original content from this work may be used under the terms of the Creative Commons Attribution 4.0 licence. Any further distribution of this work must maintain attribution to the author(s) and the title of the work, journal citation and DOI.

## 2. Observations

### 2.1. Photometric Observations

#### 2.1.1. TESS Photometry

TOI-1408 (TIC 364186197) was observed at a 2 minute cadence by TESS in Sectors 16, 17, 18, 19, 24, 25, 52, 57, 58, 59, 73, and 76 from 2019 September 12 to 2024 March 25, spanning 61 transits for TOI-1408 b and 114 transits for TOI-1408 c. We used the publicly available Presearch Data Conditioning (PDC) light curves (Smith et al. 2012; Stumpe et al. 2012, 2014) produced by the Science Processing Operations Center (SPOC; Jenkins et al. 2016) at the NASA Ames Research Center, downloaded from the Mikulski Archive for Space Telescopes.[49]

#### 2.1.2. Ground-based Photometry

*NOT/ALFOSC*—We observed five TOI-1408 b transits in the *i* band using the Alhambra Faint Object Spectrograph and Camera (ALFOSC) instrument installed at the 2.56 m Nordic Optical Telescope (NOT) at the Roque de los Muchachos Observatory on La Palma, Spain, between 2021 July 8 and 2022 August 28. The photometry was reduced with our pipeline following standard photometry practices (Parviainen et al. 2019). The reduced photometry from NOT and all the other instruments is available in Table 1.

*LCOGT/Sinistro*—We observed six TOI-1408 b transits in the *i* band using the Sinistro cameras installed at 1 m telescopes from the Las Cumbres Observatory Global Telescope (LCOGT; Brown et al. 2013) between 2021 July 21 and 2023 July 30. The photometry was reduced with the same

[49] https://mast.stsci.edu

**Table 1**
Ground-based Photometry

| time (BJD) | Flux | e_Flux | Instrument |
|---|---|---|---|
| 2459501.794176 | 1.001 | 0.002 | M3_g |
| 2459501.794335 | 1.002 | 0.002 | M3_g |
| 2459501.794457 | 0.999 | 0.002 | M3_g |
| 2459501.794579 | 1.000 | 0.002 | M3_g |
| 2459501.794702 | 0.999 | 0.002 | M3_g |
| 2459501.794824 | 1.000 | 0.002 | M3_g |

(This table is available in its entirety in machine-readable form in the online article.)

**Table 2**
RV Measurements and Their Uncertainties

| time (BJD) | RV ($m\,s^{-1}$) | e_RV ($m\,s^{-1}$) | Instrument |
|---|---|---|---|
| 2459114.650183 | −33581.2 | 12.5 | McD HJST |
| 2459115.814081 | −33383.9 | 19.8 | McD HJST |
| 2459116.786824 | −33541.8 | 16.2 | McD HJST |
| 2459133.725274 | −33413.8 | 19.9 | McD HJST |
| 2459135.701365 | −33784.5 | 22.7 | McD HJST |
| 2459143.690476 | −33627.5 | 8.7 | McD HJST |

(This table is available in its entirety in machine-readable form in the online article.)

pipeline as the NOT photometry. We also observed two transits of TOI-1408 b on 2021 May 21 and on 2022 September 11 in the Pan-STARRS $z$-short band. The $z$-short band images were calibrated by the standard LCOGT BANZAI pipeline (McCully et al. 2018), and differential photometric data were extracted using AstroImageJ (Collins et al. 2017).

*LCOGT/MuSCAT3*—We observed two transit of TOI-1408 b using the multicolor MuSCAT3 instrument (Narita et al. 2020) installed at the 2 m Faulkes Telescope North of LCOGT in Maui, Hawaii on 2021 October 14 and 2022 November 12. The transits were observed simultaneously in the $g$, $r$, $i$, and $z_s$ bands. The images were calibrated by the BANZAI pipeline (McCully et al. 2018), and aperture photometry was performed with a custom pipeline described in Fukui et al. (2011). We included only the first transit due to the low S/N of the second observation.

*Palomar/WIRC*—We observed one transit of TOI-1408 b on 2022 September 2 in the $K$-continuum band using the Wide-field Infrared Camera installed on the 5.1 m Hale Telescope at Palomar Observatory in California. We calibrated the images with the pipeline described in Vissapragada et al. (2020), and then performed aperture photometry and detrended the light curve with the procedure described in Greklek-McKeon et al. (2023).

### 2.2. Spectroscopic Observations

*HARPS-N*—We obtained 60 high-resolution spectra using the High Accuracy Radial velocity Planet Searcher-North (HARPS-N; $\lambda \in$(378–691) nm, $R \approx 115{,}000$; Cosentino et al. 2012) mounted at the 3.58 m Telescopio Nazionale Galileo of the Roque de los Muchachos Observatory in La Palma, Spain, under the observing program CAT21A_119 between 2021 May 21 and 2024 June 19. The exposure time was set to 480–1800 s based on weather conditions and scheduling constraints, leading to a signal-to-noise ratio (SNR) per pixel of 36–112 at 550 nm. The spectra were extracted using the offline version of the HARPS-N data reduction system (DRS) pipeline (Cosentino et al. 2014), version HARPN_3.7. Absolute radial velocities (RVs) were measured using an online version of the DRS, the YABI tool,[50] by cross-correlating the extracted spectra with a G2 mask (Baranne et al. 1996). The DRS RVs from HARPS-N and all other instruments can be found in Table 2.

*McDonald*—We observed 89 high-precision spectra of TOI-1408 using the McDonald Observatory 2.7 m Harlan J. Smith telescope (HJST) with its Tull Coudé spectrometer ($\lambda \in$ (340–1090) nm, $R \approx 60{,}000$; Tull et al. 1995). We pass the starlight through an $I_2$ gas absorption cell in front of the spectrograph entrance slit in order to impose our high-precision RV metric on the spectrum. We used an exposure meter to terminate each observation when an SNR of about 25–40 per pixel was achieved. All observations were reduced and 1D spectra were extracted using standard IRAF routines. We computed the RVs given in Table 2 using the AUSTRAL code (Endl et al. 2000).

*TLS*—We obtained 232 spectra of TOI-1408 using the Coudé Échelle spectrograph of the 2 m Alfred Jensch telescope of the Thüringer Landessternwarte (TLS) Tautenburg. The spectrograph's old camera (CCD3, $\lambda \in$(452–765) nm, $R = 51{,}000$) was updated to a new (Andor, $\lambda \in$(460–734) nm, $R = 63{,}000$) during the observing period. When modeling the RVs, we allowed for a velocity offset between the pre-upgrade and post-upgrade data sets because of the difference between the two cameras. We obtained 74 spectra with CCD3 and 158 spectra with the Andor-CCD with most exposure times of 1200 s. The observations were carried out using an iodine cell for wavelength calibrations. The RVs were obtained from the reduced spectra using viper (Zechmeister et al. 2021) and the co-added HARPS-N spectrum as a template.

*CAFE*—We observed 20 spectra of TOI-1408 with the Calar Alto Fiber-fed Echelle (CAFE) spectrograph ($\lambda \in$(407–925) nm, $R = 60{,}000$; Aceituno et al. 2013) mounted at the 2.2 m telescope of the Calar Alto observatory between 2021 November 10 and 2022 August 19 with a typical SNR of 30. We used the observatory pipeline described in Lillo-Box et al. (2020) to perform the basic reduction and extraction of the spectra. This pipeline also determines the RV by performing cross-correlation against a solar binary mask and correcting them from intranight drifts using the thorium–argon frames obtained in between each science frame. Usually, several epochs were obtained per night with a mean individual RV uncertainty of 17 $m\,s^{-1}$. The RVs were corrected for nightly zero-points determined by observing the same sample of RV standards every observation night.

*SOPHIE*—We observed 15 high-precision spectra of TOI-1408 with the SOPHIE échelle spectrograph ($\lambda \in$ (387–694) nm, $R = 75{,}000$) between 2020 August and 2023 August installed at the 1.93 m telescope of Observatoire de Haute-Provence, France (Perruchot et al. 2008; Bouchy et al. 2009). For each spectrum, the exposure time was between 360 s and 1020 s, providing an SNR per pixel at 550 nm between 38 and 53 depending on the weather conditions. The RVs were extracted with the standard SOPHIE pipeline using cross-correlation as presented by Bouchy et al. (2009) and refined by

[50] Available at http://ia2-harps.oats.inaf.it:8000.

Heidari et al. (2024). The derived RVs have typical uncertainties on the order of $\pm 7\,\mathrm{m\,s^{-1}}$.

*MaHPS*—We observed 61 spectra between 2022 May and October using the 2.1 m Fraunhofer Telescope at the Wendelstein Observatory (WO) in the German Alps. The Manfred Hirt Planet Spectrograph (MaHPS) comprises the high-resolution spectrograph FOCES combined with the Menlo Systems Astrofrequency comb as a calibration light source ($\lambda \in$ (380–880) nm, $R = 60{,}000$). For the data reduction from 2D to 1D, we used `GAMSE`. For the comb calibration, creation of the B-spline optimized templates, and RV extraction via a fit, we used our pipeline `MARMOT`. Descriptions of both can be found in Kellermann (2021). We provide two data sets one with Thar and one with comb calibration.

*TRES*—We obtained 18 spectra with the Tillinghast Reflector Echelle Spectrograph (TRES; $\lambda \in$(384–910) nm, $R = 44{,}000$; Fűrész 2008) mounted on the 1.5 m Tillinghast Reflector at the Fred Lawrence Whipple Observatory on Mount Hopkins in southern Arizona between 2019 December 5 and 2024 June 17. The reduction and RV analysis followed the procedures described in Buchhave et al. (2010) and Quinn et al. (2012). The main difference is that the template spectrum for the RV extraction was created by median-combining all of the out-of-transit observed spectra of TOI-1408 (after shifting to align them). Thus, these are relative velocities where the internal precision of each observation has been based on the scatter in the velocities between the individual echelle orders.

*OES*—We observed 14 spectra with the Ondrejov Echelle Spectrograph (OES; $\lambda \in$(380–900) nm, $R = 50{,}000$; Kabáth et al. 2020) installed on a 2 m Perek telescope in Ondřejov, Czech Republic. Exposure times varied from 2700 to 3600 s depending on the weather conditions. The data are reduced via standard spectroscopic IRAF routines. OES is used for the KESPRINT follow-up of TESS targets (Šubjak et al. 2020; Kabáth et al. 2022; Tran et al. 2022).

*HERMES*—We monitored the system for ten days in 2020 August with the High Efficiency and Resolution Mercator Echelle Spectrograph (HERMES; $\lambda \in$(375–900) nm, $R = 90{,}000$; Raskin et al. 2011), mounted on the 1.2 m Mercator telescope at the Spanish Observatorio del Roque de los Muchachos of the Instituto de Astrofísica de Canarias. We obtained these observations with simultaneous thorium–argon emission spectra, which allows for a precision of 2–3 $\mathrm{m\,s^{-1}}$ (Beck et al. 2015).

## 3. Analysis

### 3.1. Stellar Characterization

We carried out a stellar analysis using the co-added HARPS-N spectra following an approach described in Fridlund et al. (2017) and Persson et al. (2018) using the empirical `SpecMatch-Emp` code (Yee et al. 2017) and the Spectroscopy Made Easy (`SME`) analysis package (Valenti & Piskunov 1996; Piskunov & Valenti 2017) version 5.22 to obtain the effective temperature, $T_{\rm eff}$, the logarithm of the surface gravity, $\log g$, $V \sin i_\star$, and the abundance of iron relative to hydrogen, [Fe/H]. The derived stellar parameters from `SME` were used to model the stellar radius and mass with the spectral energy distribution Bayesian model averaging fitter (`ARIADNE`; Vines & Jenkins 2022) using the `Phoenix v2` (Husser et al. 2013), `BtSettl` (Allard et al. 2012), Castelli & Kurucz (2003), and Kurucz (1979) atmospheric model grids. The stellar rotation period, estimated from the spectroscopically derived $V \sin i_\star$ and the stellar radius assuming that the star is seen equator-on, is $7.9 \pm 0.6$ days. This period is also identified from the TESS photometry with a Lomb–Scargle periodogram as well as by running the rotation pipeline (Mathur et al. 2010; García et al. 2014; Santos et al. 2021) on the Quick Look Pipeline (Huang et al. 2020b) data, we derived a rotation period of $7.5 \pm 0.62$ days, indicating that the planetary orbital axis is indeed well-aligned with the spin of the star. This supports a more quiet formation scenario, such as disk migration. The results from the models are listed in Table 3 alongside further stellar properties.

**Table 3**
Stellar Parameters of TOI-1408

| Parameter | Value | Reference |
|---|---|---|
| R.A. [J2000, epoch 2016] | 20:54:02.653 | (1) |
| Decl. [J2000, epoch 2016] | +72:34:50.34 | (1) |
| parallax [mas] | $7.16 \pm 0.01$ | (1) |
| $\mu_{\alpha\star}$ [mas yr$^{-1}$] | $11.85 \pm 0.01$ | (1) |
| $\mu_{\delta\star}$ [mas yr$^{-1}$] | $28.73 \pm 0.01$ | (1) |
| RUWE | 0.88 | (1) |
| Distance [pc] | $139.13 \pm 0.2$ | (1) |
| $V$ [mag] | $9.27 \pm 0.02$ | (2) |
| $J$ [mag] | $8.37 \pm 0.02$ | (3) |
| Spectral type | F8 V | this work |
| Age [Gyr] | $2.7 \pm 0.3$ | this work |
| $T_{\rm eff}$ [K] | $6117 \pm 31$ | this work |
| [Fe/H] [dex] | $0.25 \pm 0.06$ | this work |
| $\log g$ [cm s$^{-2}$] | $4.10 \pm 0.06$ | this work |
| $V \sin i_\star$ [km s$^{-1}$] | $9.8 \pm 0.7$ | this work |
| $M_\star$ [$M_\odot$] | $1.31 \pm 0.01$ | this work |
| $R_\star$ [$R_\odot$] | $1.53 \pm 0.02$ | this work |
| $\rho_\star$ [g cm$^{-3}$] | $0.51 \pm 0.02$ | this work |
| $L_\star$ [$L_\odot$] | $2.96 \pm 0.10$ | this work |

**References.** 1: Gaia DR3 (Gaia Collaboration et al. 2016; Babusiaux et al. 2023; Gaia Collaboration et al. 2023), 2: Tycho-2 (Høg et al. 2000), 3: Two Micron All Sky Survey (Cutri et al. 2003).

### 3.2. Discovery of TOI-1408 c

A TTV search using Python Tool for Transit Variation (`PyTTV`; Korth et al. 2023) revealed a clear TTV signal for TOI-1408 b, suggesting the presence of an additional body in the TOI-1408 system. We used the Open Transit Search pipeline (`OpenTS`; Pope et al. 2016) to search for additional transit signals from the TESS Sectors 16, 17, 18, 19, 24, and 25. This analysis identified a transit-like signal with a period of 2.22 days, a depth of 100 ppm, and a transit duration of 0.62 hr. This signal has not been reported as a TOI by the TESS mission. We also identified the transiting signal using the Détection Spécialisée de Transits code (Cabrera et al. 2012).

Following the detection of the tentative transit signal, we carried out a dynamical stability analysis using `Rebound` (Rein & Liu 2012), which confirmed that the orbits are compatible with long-term stability and predicted large TTVs. Further analysis of individual TESS sectors supported the existence of large TTVs for TOI-1408 c. The transit durations and depths estimated from single sectors differed from those estimated by combining multiple sectors, leading to the smearing of the transit shape. The orbital period was estimated to vary between 2.18 and 2.22 days from sector to sector. The

individual transits have too low SNR to measure their transit durations, but we estimated the average transit durations combining two TESS sectors. Sectors 16 and 17 yield an average transit duration of 2.75 hr, while Sectors 73 and 76 yield an average transit duration of 2.42 hr.

After our detection, the SPOC conducted an independent multisector transit search of the light curves up to Sector 59, using an adaptive, noise-compensating matched filter (Jenkins 2002; Jenkins et al. 2010, 2020). The 4.42 days signal of TOI-1408 b was identified with a high significance, and after removing TOI-1408 b's transits, the next strongest signal ($8.16\sigma$) had an orbital period of ~2.22 days. Despite exceeding the $7.1\sigma$ threshold, this detection was vetoed by the transit search pipeline's $\chi^2$ discriminator (Seader et al. 2013), likely due to smearing from large TTVs.

### 3.3. RVs

We carried out a two-planet RV analysis using all the RV data described in Section 3.3 with `PyTransit`'s `RVLPF` RV modeling class (Parviainen 2015). This code models the RV signals from two planets, incorporating an additional free RV offset and jitter term for each RV data set, a sinusoidal stellar rotational signal, and a quadratic trend in time to account for possible long-period companions. An analysis with wide normal priors on the planet b and c periods and transit centers identified with `OpenTS` leads to a posterior period estimate of $2.1613 \pm 0.0002$ days and an RV semi-amplitude of $5.0 \pm 1.0\,\mathrm{m\,s^{-1}}$ that corresponds to a minimum mass of $13.0 \pm 3.0\,M_{\oplus}$. The RV information about TOI-1408 c comes from the HARPS-N data combining high precision with a long observing time span. For TOI-1408 b, we obtain a close-to-circular orbit with an RV semi-amplitude of $191.3 \pm 0.9\,\mathrm{m\,s^{-1}}$, translating to a minimum planet mass of $1.846 \pm 0.009\,M_{\mathrm{Jup}}$.

The RV analysis also detected a clear nonlinear trend showing evidence of an outer companion with an orbital period of thousands of days. Including the first two TRES points observed ~200 days before the main observing campaign started gives a Keplerian orbit with a period of ~2530 days with $K = 195 \pm 4\,\mathrm{m\,s^{-1}}$, $M_{\mathrm{p}} = 14.6 \pm 0.3\,M_{\mathrm{Jup}}$, and an eccentricity of $0.35 \pm 0.02$. However, since the two points responsible for the solution are separated from the rest, we leave the characterization of the outer planet as future work requiring significantly longer RV follow-up.

Gaia Data Release (DR) 3 astrometry indicates that the source is a primary star with 25 visibility periods and a ruwe of 0.88, indicating the solution is a good fit for linear space motion. At first sight, this would indicate it is a single star (Gaia astrometry could not detect planets with periods of a few days). However, the astrometry also shows an excess noise of 0.062 mas with a high significance of 4.7, which indicates there is a significant but small disturbance remaining. Gaia DR3 uses 34 months of data and may be sampling a substantial fraction of the suggested orbital period; however, very long orbital periods would require much more than 34 months of data to detect a companion.

We can estimate the astrometric signature of the long-period outer companion using the parameters given in this Letter and assuming an almost circular orbit. The period can be used to estimate a semimajor axis for a roughly circular orbit, and the astrometric signature is obtained using

$$\alpha = \left(\frac{M_p}{M_\star}\right)\left(\frac{a_p}{1\ \mathrm{au}}\right)\left(\frac{d}{1\ \mathrm{pc}}\right)\ [\mathrm{arsec}]. \quad (1)$$

The suspected third planet gives an astrometric signature of 0.364 mas, which should be easily detectable by Gaia, but with a period of almost 7 yr compared to the Gaia mission duration of only 2.8 yr, it could remain undetected until Gaia DR4 or DR5, especially if the planet is near apogee or if its period is underestimated.

### 3.4. Photodynamical Analysis

Since the planets strongly interact gravitationally, producing significant TTVs, we performed a photodynamical analysis by modeling the TESS photometry, the ground-based photometry, and the ground-based RVs from various facilities. This was done using `PyTTV` following the approach described in Korth et al. (2023). We assumed a two-planet model, a sinusoidal RV signal to account for the stellar rotation based on the results from the stellar characterization in Section 3.1, and a quadratic RV trend based on the results from the RV analysis in Section 3.3. The model is parametrized as described in Korth et al. (2023), with the exception of the impact parameter, $b$. Instead, we used the grazing parameter, $g = b/(1+k)$, where $k$ is the radius ratio, due to the grazing geometry of TOI-1408 b. The longitudes of the ascending notes, $\Omega$, are fixed to $\pi$ for both planets. The model is parameterized using the sampling parameters $\sqrt{e}\cos\omega$ and $\sqrt{e}\sin\omega$, but we also set a prior on the orbital eccentricities. The model parameters and their priors are listed in Table 4.

The code models the photometry and RVs simultaneously using `Rebound` (Rein & Liu 2012; Rein & Spiegel 2015; Tamayo et al. 2020) for dynamical integration, including general relativity effects as implemented in `Reboundx` (Tamayo et al. 2020) and `PyTransit` (Parviainen 2015; Parviainen & Korth 2020; Parviainen 2020) for transit modeling. The analysis begins with a global optimization using the differential evolution method (Storn & Price 1997; Price et al. 2005), followed by Markov Chain Monte Carlo sampling starting from the global optimization results with the `emcee` sampler (Foreman-Mackey et al. 2013).

We show the TESS photometry and RV measurements with their corresponding model in Figure 1, the ground-based photometry in Appendix A, the TTV model in Figure 2, and the full RV model in Appendix B. The posteriors for model parameters and the derived planetary parameters are listed in Table 4. The posterior mean ephemeris for TOI-1408 c is $T_{0,c} = 2458739.845 \pm 0.002$ days and $P_c = 2.19592 \pm 0.00002$ days, while for TOI-1408 b, the ephemeris is $T_{0,b} = 2458740.8584 \pm 0.0002$ days and $P_b = 4.424703 \pm 0.000001$ days. TOI-1408 c exhibits a TTV period of 138 days with an amplitude of 8 hr, and TOI-1408 b shows TTVs with an amplitude of 8 minutes. TOI-1408 c's TTV amplitude is 15% of its orbital period, the largest TTV amplitude relative to a planet's orbital period known at the time of writing. The transit duration variations (TDVs) for TOI-1408 c calculated from the photodynamical model agree with the measured values.

In a previous study by Galazutdinov et al. (2023), TOI-1408 b was found to have a mass of $1.69 \pm 0.20\,M_{\mathrm{Jup}}$ and an eccentric orbit ($e = 0.259 \pm 0.026$). While their mass value agrees within $1\sigma$ with our (largely more precise) value of $1.86 \pm 0.02\,M_{\mathrm{Jup}}$, we find TOI-1408 b's orbit to be nearly circular. Additionally, our photodynamical modeling could constrain TOI-1408 b's radius more reliably.

**Table 4**
Photodynamical Model Parameters with Their Priors and Posteriors, and the Posteriors for Derived Planetary Parameters

| *Stellar Parameter* | Prior | Posterior |
|---|---|---|
| $R_\star$ [$R_\odot$] | $\mathcal{N}(1.534, 0.021)$ | $1.53 \pm 0.02$ |
| $M_\star$ [$M_\odot$] | $\mathcal{N}(1.309, 0.012)$ | $1.312 \pm 0.009$ |
| Limb darkening $q_1$ | $\mathcal{U}(0, 1)$ | $0.5 \pm 0.1$ |
| Limb darkening $q_2$ | $\mathcal{U}(0, 1)$ | $<0.85$[a] |
| $\rho_\star$ [g cm$^{-3}$] | ⋯ | $0.52 \pm 0.02$ |
| *RV parameter* | | |
| $\gamma$ [m s$^{-1}$] | $\mathcal{N}$[b] | ⋯ |
| $\dot{\gamma}$ [m s$^{-1}$ day$^{-1}$] | $\mathcal{N}(0, 1)$ | $-0.344 \pm 0.002$ |
| $\ddot{\gamma}$ [m s$^{-1}$ day$^{-2}$] | $\mathcal{N}(0.000, 0.001)$ | $0.000143 \pm 0.000004$ |
| $\log_{10}$ RV jitter [$\log_{10}$ m s$^{-1}$] | $\mathcal{N}$[c] | ⋯ |
| $P_{\rm rot}$ [days] | $\mathcal{N}(7.90, 0.05)$ | $7.91 \pm 0.02$ |
| $A_{\rm rot}$ [m s$^{-1}$] | $\mathcal{U}(0, 40)$ | $2.3 \pm 0.7$ |

| | TOI-1408 c | | TOI-1408 b | |
|---|---|---|---|---|
| *Fitted planet parameter* | Prior | Posterior | Prior | Posterior |
| $P$ [days] | $\mathcal{N}(2.170, 0.005)$ | $2.1664 \pm 0.0001$ | $\mathcal{N}(4.424, 0.005)$ | $4.42587 \pm 0.00003$ |
| $T_0$ [BJD] | $\mathcal{N}(2458739.84, 0.01)$ | $2458739.847 \pm 0.004$ | $\mathcal{N}(2458740.85, 0.01)$ | $2458740.8581 \pm 0.0002$ |
| $\log_{10} M_{\rm p}$ [$\log_{10} M_\odot$] | $\mathcal{U}(-5.3, -3.9)$ | $-4.64 \pm 0.01$ | $\mathcal{N}(-2.7, 0.03)$ | $-2.749 \pm 0.003$ |
| $R_{\rm p}/R_\star$ | $\mathcal{N}(0.014, 0.004)$ | $0.0134 \pm 0.0003$ | $\mathcal{U}(0.05, 0.35)$ | $0.15 \pm 0.02$ |
| $\sqrt{e}\cos\omega$ | $\mathcal{U}(-0.5, 0.5)$ | $-0.353 \pm 0.0005$ | $\mathcal{U}(-0.5, 0.5)$ | $0.012 \pm 0.007$ |
| $\sqrt{e}\sin\omega$ | $\mathcal{U}(-0.5, 0.5)$ | $0.103 \pm 0.002$ | $\mathcal{U}(-0.5, 0.5)$ | $-0.046 \pm 0.006$ |
| $g$ | $\mathcal{U}(0, 1)$ | $0.73 \pm 0.02$ | $\mathcal{U}(0, 1)$ | $0.939 \pm 0.004$ |
| *Derived planet parameter* | | | | |
| $M_{\rm p}$ [$M_\oplus$] | ⋯ | $7.6 \pm 0.2$ | ⋯ | $593 \pm 4$ |
| $R_{\rm p}$ [$R_\oplus$] | ⋯ | $2.22 \pm 0.06$ | ⋯ | $25 \pm 4$ |
| $\rho_{\rm p}$ [g cm$^{-3}$] | ⋯ | $3.8 \pm 0.3$ | ⋯ | $0.18^{+0.17}_{-0.08}$ |
| $T_{14}$ [h] | ⋯ | $2.67 \pm 0.06$ | ⋯ | $1.65 \pm 0.03$ |
| $e$ | $\mathcal{N}(0, 0.083)$ | $0.1353 \pm 0.0001$ | $\mathcal{N}(0, 0.083)$ | $0.0023 \pm 0.0005$ |
| $\omega$ [°] | ⋯ | $286.3 \pm 0.3$ | ⋯ | $170 \pm 10$ |
| $i$ [°] | ⋯ | $82.6 \pm 0.3$ | ⋯ | $82.4 \pm 0.2$ |
| $a/R_\star$ | ⋯ | $5.04 \pm 0.06$ | ⋯ | $8.13 \pm 0.09$ |
| $a$ [au] | ⋯ | $0.03587 \pm 0.00008$ | ⋯ | $0.05778 \pm 0.0001$ |

**Notes.** $\mathcal{N}(\mu, \sigma)$ stands for a normal prior with a mean $\mu$ and standard deviation $\sigma$, and $\mathcal{U}(a, b)$ stands for a uniform distribution from $a$ to $b$. The osculating orbital elements are valid for the reference time $T_0 = 2458739.84$.
[a] The $q_2$ limb-darkening coefficient is not well constrained so we give only its 99th percentile upper limit.
[b] The instrument-specific RV shifts, $\gamma$, have loosely informative priors based on the RV measurement medians and scatters.
[c] All RV jitter terms have the same prior $\mathcal{N}(-1, 1)$.

## 4. Discussion

### 4.1. Dynamics

Besides the large TTVs, TOI-1408 c also exhibits TDVs. Forward modeling of the posterior solution from Table 4 allowed us to identify three main contributions to the TDVs, similar to those observed in KOI-142 (Nesvorný et al. 2013). The largest contribution arises from the variability in $e\cos\omega$ with a period of ∼1 yr and a peak-to-peak (ptp) amplitude of 0.4 hr. The second largest contribution is due to variations in the orbital inclination, with a period of ∼15 yr and a ptp amplitude of 0.2 hr. The third contribution comes from the variation in the tangential velocity mid-transit, which has a period similar to the TTV period and a ptp amplitude of 0.08 hr.

The two planets of TOI-1408 lie close to the 2:1 period commensurability ($P_{\rm b}/P_{\rm c} \approx 2.04$), raising the question of whether the system is dynamically in resonance. We first checked for libration of the resonant argument of the lower-mass interior planet $\theta_{\rm c} = 2\lambda_{\rm b} - \lambda_{\rm c} - \varpi_{\rm c}$. This resonant argument shows libration of about 0°, suggesting a resonant state (Figure 3, left). To understand the resonant dynamics more deeply, we then compared the system's behavior to the Hamiltonian resonance model of Nesvorný & Vokrouhlický (2016). The resonant argument in this model still librates (about 180°), but when we examine the full phase portrait, the resonant separatrix does not exist (Figure 3, right). The separation to resonance, quantified by the parameter $\delta$ of Nesvorný & Vokrouhlický (2016), is around $\delta = 0.3$ for all posterior draws (mean $\delta = 0.297$ with a standard deviation of 0.002). The resonant separatrix exists only for $\delta \geqslant 1$, and hence this system is by this definition just wide of resonance, similar to KOI-142 and TOI-2202 (Nesvorný et al. 2022). This could imply that convergent migration in the protoplanetary disk did not proceed far enough to drive the system deeply into resonance, or alternatively, that tidal forces or other effects caused the orbits to diverge and escape from the resonant state (Delisle et al. 2012).

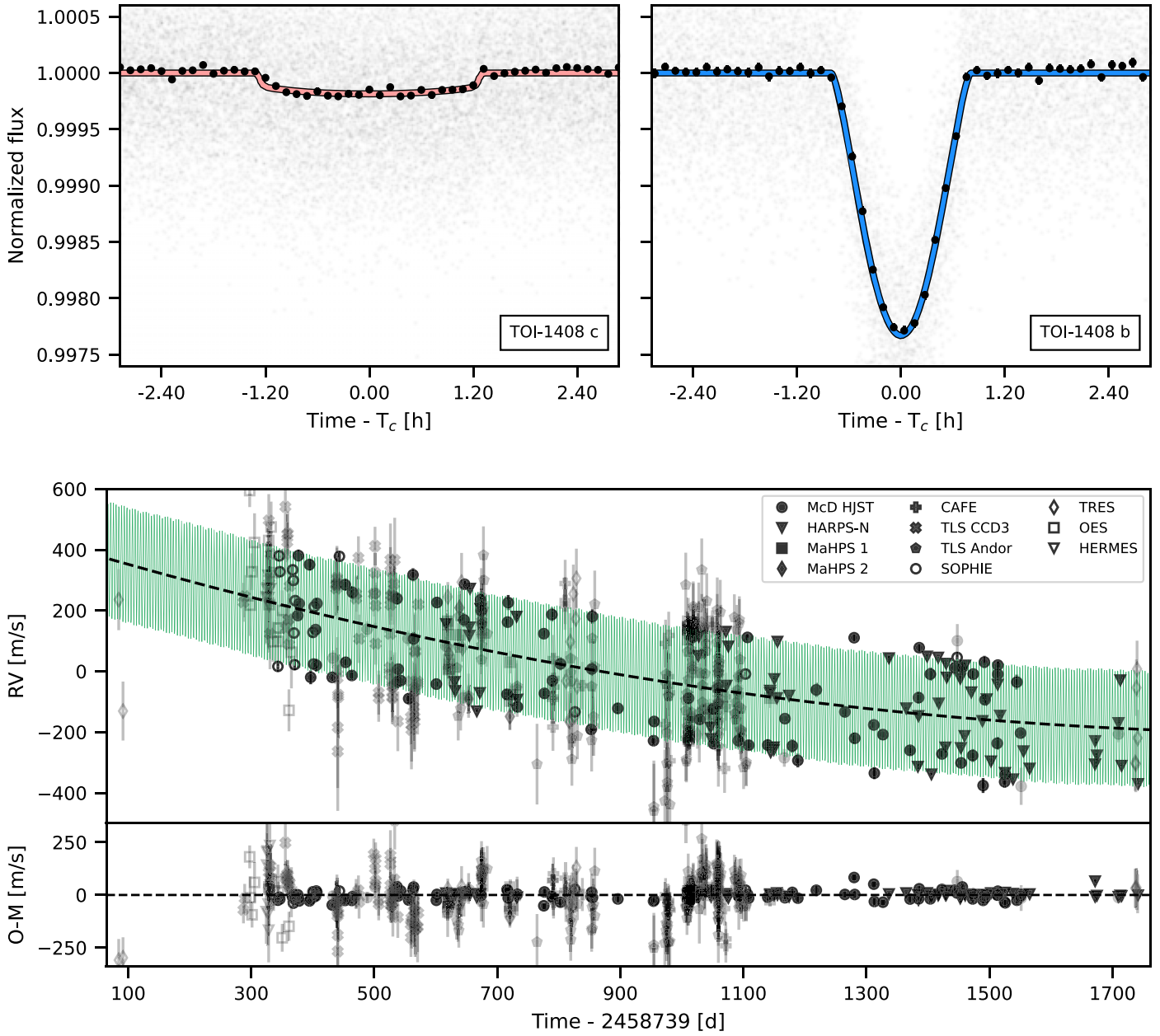


**Figure 1.** Photometry from TESS (top) and the RV measurements from different instruments (bottom) with the posterior models from the photodynamical analysis. The photometry is centered around the transit centers, with light gray points showing the raw photometry and black points with error bars showing the photometry binned to 7 minutes. The RV figure shows the RV observations as black symbols with error bars, the photodynamical RV model as a green line, and the quadratic trend as a black dashed line. The gray symbols mark observations with uncertainties >25 m s$^{-1}$, and the black symbols observations with uncertainties <25 m s$^{-1}$. See Figure 5 in Appendix A for the ground-based photometry of TOI-1408 b and Figure 6 in Appendix B for a detailed illustration of the RV observations and the RV model.

### 4.2. Stability

We performed a numerical stability analysis using `Rebound` and its implementation of the Mean Exponential Growth factor of Nearby Orbits (MEGNO; Cincotta & Simó 2000) indicator to determine if the planetary system lies in a stable configuration, which we define as $|\mathrm{MEGNO} - 2| < 0.4$. We mapped the system's stability in the $P_b - P_c$, and $e_c - P_c$ parameter spaces by drawing samples from the photodynamical model posterior and replacing the mapped parameters with samples created using a quad-tree-based importance sampler. We simulated the system for 1.6 million TOI-1408 c orbits for each sample using the WHFast integrator (Rein & Tamayo 2015) and saved the MEGNO indicator. We visualize the results as a stability map shown in Figure 4, where the value of a cell represents the fraction of stable orbits within that cell. It is worth noting that the system is close to a narrow zone of instability.

### 4.3. Implications from Occurrence Rates

The results highlight the unique position of TOI-1408 as a stable island in a chaotic environment, particularly given the low occurrence rate of inner companions to HJs, estimated at $1.4\% \pm 1.0\%$ by He et al. (2024). Their findings, based on $N$-body simulations spanning a period of $10^8$ yr, agree with the lower limit from a previous study by Wu et al. (2023), which reported a rate of nonaligned nearby planetary companion to

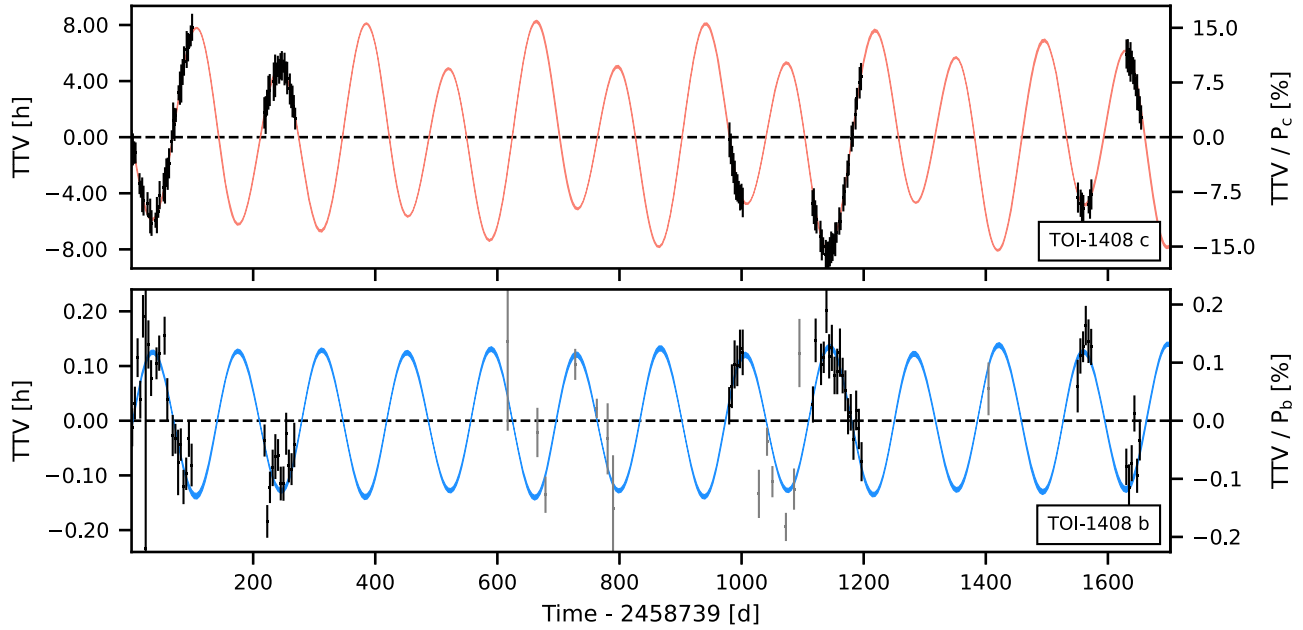


**Figure 2.** Posterior TTV model from the photodynamical modeling of TOI-1408 c (upper panel) and TOI-1408 b (lower panel). The colored lines span the 0.5 to 99.5 percentiles of the TTV model posterior distribution from the photodynamical analysis, but the uncertainties are mostly smaller than the line width. The dashed lines mark the subtracted mean orbital periods and the TTVs with their individual uncertainties measured by fitting each transit center separately are shown as black (TESS) and gray (ground-based) points with error bars for comparison.

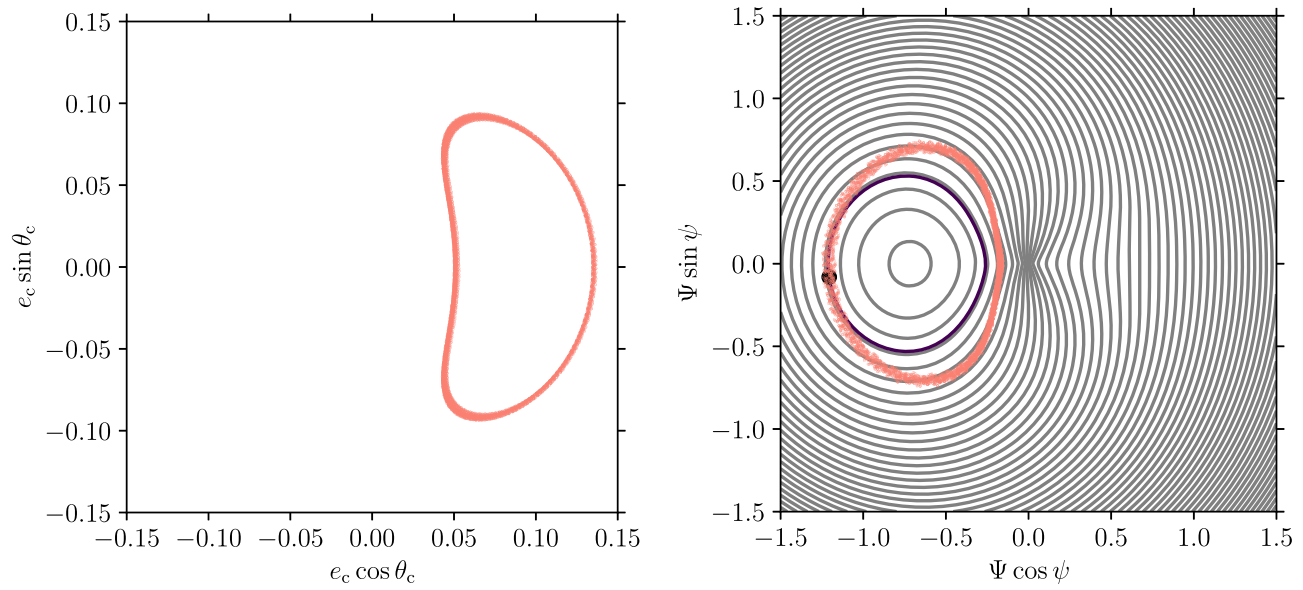


**Figure 3.** Resonant behavior of the TOI-1408 b–c pair. Left: behavior of the single-planet resonant argument, $\theta_c$, from the photodynamical simulations, showing libration about zero. Right: the same solution, transformed to the canonical resonance model of Nesvorný & Vokrouhlický (2016), where $\Psi$ is a function of both planets' eccentricities, and $\psi$ of both planets' resonant arguments, although both are dominated by inner planet c. This numerical solution is marked in salmon, and $\psi$ librates about $\pi$. However, a comparison to level curves of the Hamiltonian (gray, with black marking the analytical curve corresponding to the numerical solution) shows that no resonant separatrix exists for these system parameters.

hot Jupiters at $12\% \pm 6\%$ based on a search for TTVs in the Kepler sample. He et al. (2024) also found that the occurrence rate of inner companions to HJ significantly decreases as the HJ's orbital period shortens, resulting in only a few stable systems with HJ orbital periods of less than 6 days.

## 5. Conclusions

In this study, we report the discovery and photodynamical characterization of TOI-1408 c, a transiting sub-Neptune on a 2.2 days orbit located interior to a transiting hot Jupiter, TOI-1408 b ($P = 4.42$ days, $M = 1.86 \pm 0.02\, M_{\rm Jup}$, $R = 2.4 \pm 0.5\, R_{\rm Jup}$). The planets are near a 2:1 period commensurability with librating resonant arguments, yet both remain outside the resonant configuration. This configuration leads to remarkable TTVs and TDVs, with TOI-1408 c exhibiting the largest TTV amplitude relative to its orbital period recorded thus far.

The existence of a small inner planet in such a tight orbit around a hot Jupiter adds a valuable data point against the backdrop of current planet formation theories, challenging the typical scenarios suggested for close-in giant planets. The planets in the TOI-1408 system are both transiting and exhibit

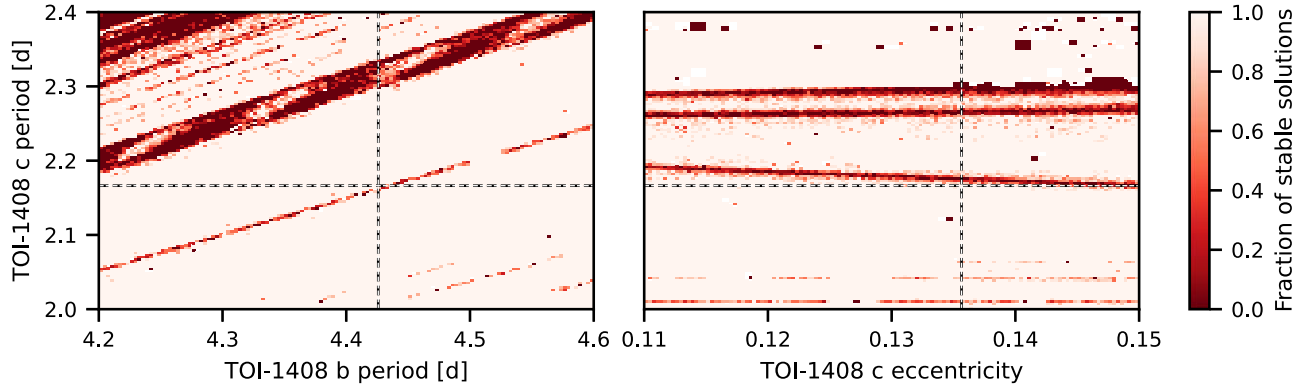


**Figure 4.** Two-dimensional MEGNO maps probing the stability near the posterior solution from the photodynamical analysis. The color indicates the orbital stability, and the dashed lines show the parameter posterior median values listed in Table 4.

measurable TTVs, similar to TOI-1130, but in a much tighter orbit configuration.

Additionally, RV measurements suggest a third, long-period outer body in the system, indicating a complex dynamical environment, such as WASP-47 and WASP-132. The system's dynamic nature and the likely presence of a third body invite further observational campaigns to refine the orbital parameters and investigate long-term stability.

This research not only deepens our understanding of multiplanet systems involving hot Jupiters with inner low-mass companions but also underscores the need for continued exploration to uncover the diverse architectures of exoplanetary systems.

## Acknowledgments

We thank the anonymous referee for the timely and positive feedback. This work was supported by the KESPRINT collaboration, an international consortium devoted to the characterization and research of exoplanets discovered with space-based missions (https://kesprint.science/). This Letter includes data collected with the TESS mission, obtained from the MAST data archive at the Space Telescope Science Institute (STScI). The specific data can be obtained here: doi: 10.17909/en2q-wj40. Funding for the TESS mission is provided by the NASA Explorer Program. STScI is operated by the Association of Universities for Research in Astronomy, Inc., under NASA contract NAS 5-26555. We acknowledge the use of public TESS Alert data from pipelines at the TESS Science Office and the TESS Science Processing Operations Center. Resources supporting this work were provided by the NASA High-End Computing (HEC) Program through the NASA Advanced Supercomputing (NAS) Division at Ames Research Center for the production of the SPOC data products. Based on observations made with the Nordic Optical Telescope, owned in collaboration by the University of Turku and Aarhus University, and operated jointly by Aarhus University, the University of Turku and the University of Oslo, representing Denmark, Finland and Norway, the University of Iceland and Stockholm University at the Observatorio del Roque de los Muchachos, La Palma, Spain, of the Instituto de Astrofisica de Canarias. The data presented here were obtained [in part] with ALFOSC, which is provided by the Instituto de Astrofisica de Andalucia (IAA) under a joint agreement with the University of Copenhagen and NOT. This Letter is based on observations made with the LCOGT telescopes, one of whose nodes is located at the Observatorios de Canarias del IAC on the island of Tenerife in the Observatorio del Teide. This Letter is based on observations made with the MuSCAT3 instrument, developed by the Astrobiology Center and under financial support by JSPS KAKENHI (JP18H05439) and JST PRESTO (JPMJPR1775), at Faulkes Telescope North on Maui, HI, operated by the Las Cumbres Observatory. This research has made use of the Exoplanet Follow-up Observation Program (ExoFOP; NExScI 2022) website, which is operated by the California Institute of Technology, under contract with the National Aeronautics and Space Administration under the Exoplanet Exploration Program. This Letter includes data taken at The McDonald Observatory of The University of Texas at Austin. Based on observations made with the Italian Telescopio Nazionale Galileo (TNG) operated on the island of La Palma by the Fundación Galileo Galilei of the INAF (Istituto Nazionale di Astrofisica) at the Spanish Observatorio del Roque de los Muchachos of the Instituto de Astrofisica de Canarias under programs CAT19A_162, ITP19_1, and A41TAC_49. Based partly on observations collected at the Centro Astronómico Hispano en Andalucía (CAHA) at Calar Alto, operated jointly by Junta de Andalucía and Consejo Superior de Investigaciones Científicas (IAA-CSIC). This work has made use of data from the European Space Agency (ESA) mission Gaia (https://www.cosmos.esa.int/gaia), processed by the Gaia Data Processing and Analysis Consortium (DPAC; https://www.cosmos.esa.int/web/gaia/dpac/consortium). Funding for the DPAC has been provided by national institutions, in particular, the institutions participating in the Gaia Multilateral Agreement. J.K. gratefully acknowledges the support of the Swedish National Space Agency (SNSA; DNR 2020-00104) and of the Swedish Research Council (VR: Etableringsbidrag 2017-04945) H.P. acknowledges support from the Spanish Ministry of Science and Innovation with the Ramon y Cajal fellowship No. RYC-2021-031798-I, and funding from the University of La Laguna and the Spanish Ministry of Universities. A.J.M. acknowledges financial support from the Swedish National Space Agency (Career grant 2023-00146). We acknowledge financial support from the Agencia Estatal de Investigación of the Ministerio de Ciencia e Innovación (MCIN/AEI, DOI:10.13039/501100011033) and the ERDF "A way of making Europe" through project PID2021-125627OB-C32, and from the Center of Excellence "Severo Ochoa" award to the Instituto de Astrofisica de Canarias. Also from MCIN/AEI, H.J.D.

acknowledges funding under grant PID2019-107061GB-C66 and G.M. under the Severo Ochoa grant CEX2021-001131-S and the Ramón y Cajal grant RYC2022-037854-I. J.L-B. acknowledges financial support received from "la Caixa" Foundation (ID 100010434) and from the European Unions Horizon 2020 research and innovation program under the Marie Slodowska-Curie grant agreement No. 847648, with fellowship code LCF/BQ/PI20/11760023. This research has also been partly funded by the Spanish State Research Agency (AEI) Project Nos. PID2019-107061GB-C61 and MDM-2017-0737 Unidad de Excelencia "María de Maeztu"- Centro de Astrobiología, CSIC/INTA. G.N. thanks for the research funding from the Ministry of Education and Science program the "Excellence Initiative - Research University" conducted at the Center of Excellence in Astrophysics and Astrochemistry of the Nicolaus Copernicus University in Toruń Poland. This work is partly supported by JSPS KAKENHI grant Nos. JP24H00017, JP24H00248, JP24K00689, JP24K17082, and JSPS Bilateral Program No. JPJSBP120249910. P.G.B. acknowledges support from the Spanish Ministry of Science and Innovation with the *Ramón y* Cajal fellowship Nos. RYC-2021-033137-I and MRR4032204. E.M. acknowledges funding from FAPEMIG under project No. APQ-02493-22 and a research productivity grant No. 309829/2022-4 awarded by CNPq, Brazil. D.G. gratefully acknowledges the financial support from the grant for internationalization (GAND_GFI_23_01) provided by the University of Turin. M.S. acknowledges the support of the Italian National Institute of Astrophysics (INAF) through the project "The HOT-ATMOS Project: characterizing the atmospheres of hot giant planets as a key to understand the exoplanet diversity" (1.05.01.85.04). J.Š. acknowledges the support from GACR grant 23-06384O. P.K. and M.S. are thankful for the support from grant LTT-20015. P. C. acknowledges the DFG through grant CH 2636/1-1 and the support of the Department of Atomic Energy, Government of India. E.W.G acknowledges support from the Thüringer Ministerium für Wirtschaft, Wissenschaft und Digitale Gesellschaft. R.A.G. and D.B.P. acknowledge the support from the PLATO CNES grant. S.M. acknowledges support from the Spanish Ministry of Science and Innovation with grant No. PID2019-107061GB-C66 and through AEI under the Severo Ochoa Centres of Excellence Programme 2020–2023 (CEX2019-000920-S).

*Facilities:* NOT, CTIO: 1.3 m, CTIO: 1.5 m, CXO, LCOGT, Hale, TNG, Smith, TLS, CAO: 2.2 m, OHP: 1.93 m, WO: 2 m, FLWO: 1.5 m, OO: 2, Mercator: 1.2 m.

*Software:* PyTTV (Korth et al. 2023), PyTransit (Parviainen 2015), Rebound (Rein & Liu 2012), LDTk (Parviainen & Aigrain 2015), emcee (Foreman-Mackey et al. 2013), AstroImageJ (Collins et al. 2017), TAPIR (Jensen 2013), Astropy (Astropy Collaboration et al. 2013, 2018, 2022), NumPy (Van Der Walt et al. 2011), SciPy (Virtanen et al. 2020), matplotlib (Hunter 2007).

## Appendix A
## Ground-based Transits for TOI-1408 b

We show the ground-based transits for TOI-1408 b with the photodynamical model in Figure 5.

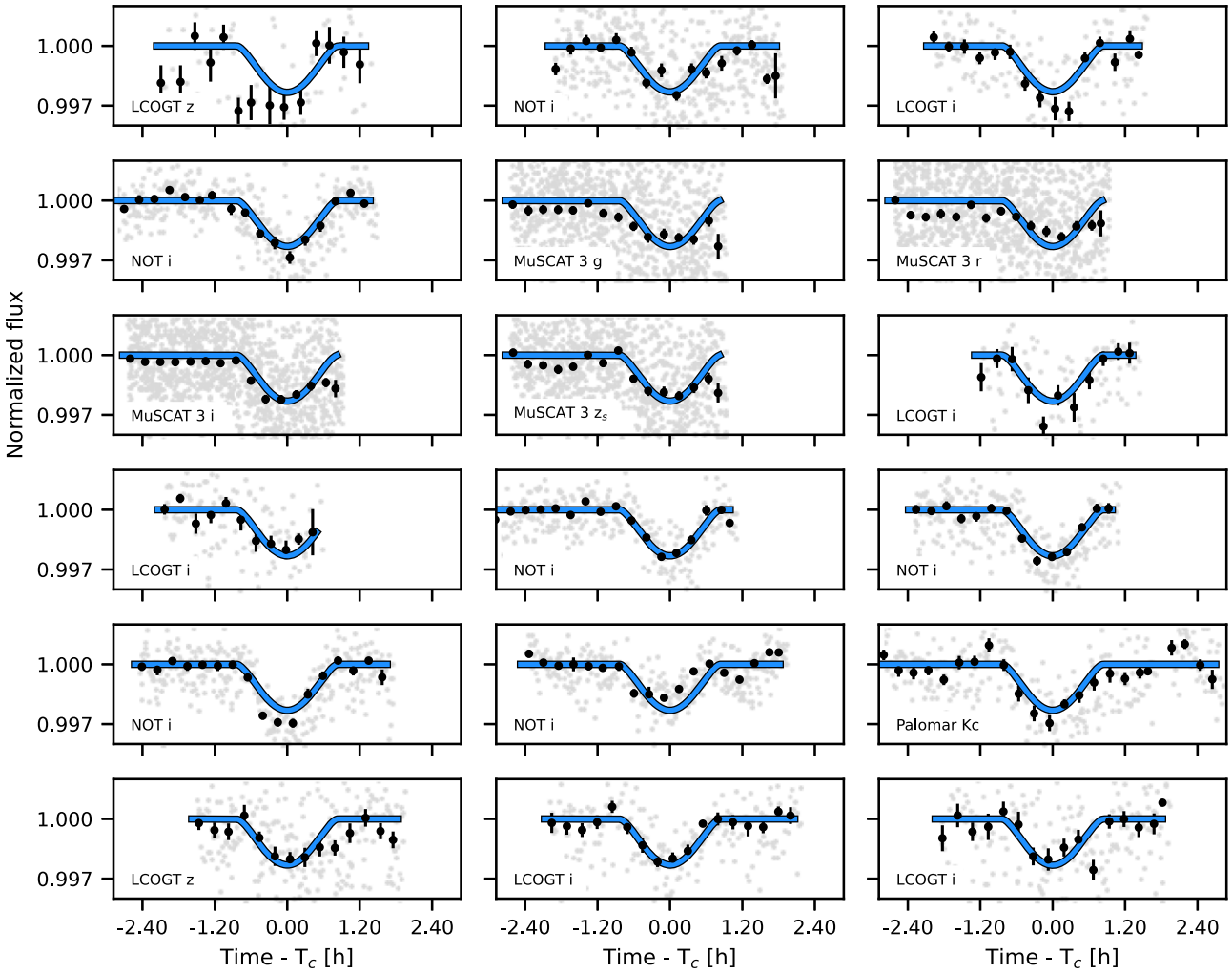


**Figure 5.** Ground-based transit measurements observed with the different facilities shown as gray points, the same points binned to 15 minutes as black points with error bars, and the photodynamical model in blue.

## Appendix B
## RV Model from the Photodynamical Analysis

We show the ground-based RV measurements for TOI-1408 system with the photodynamical model in Figure 6.

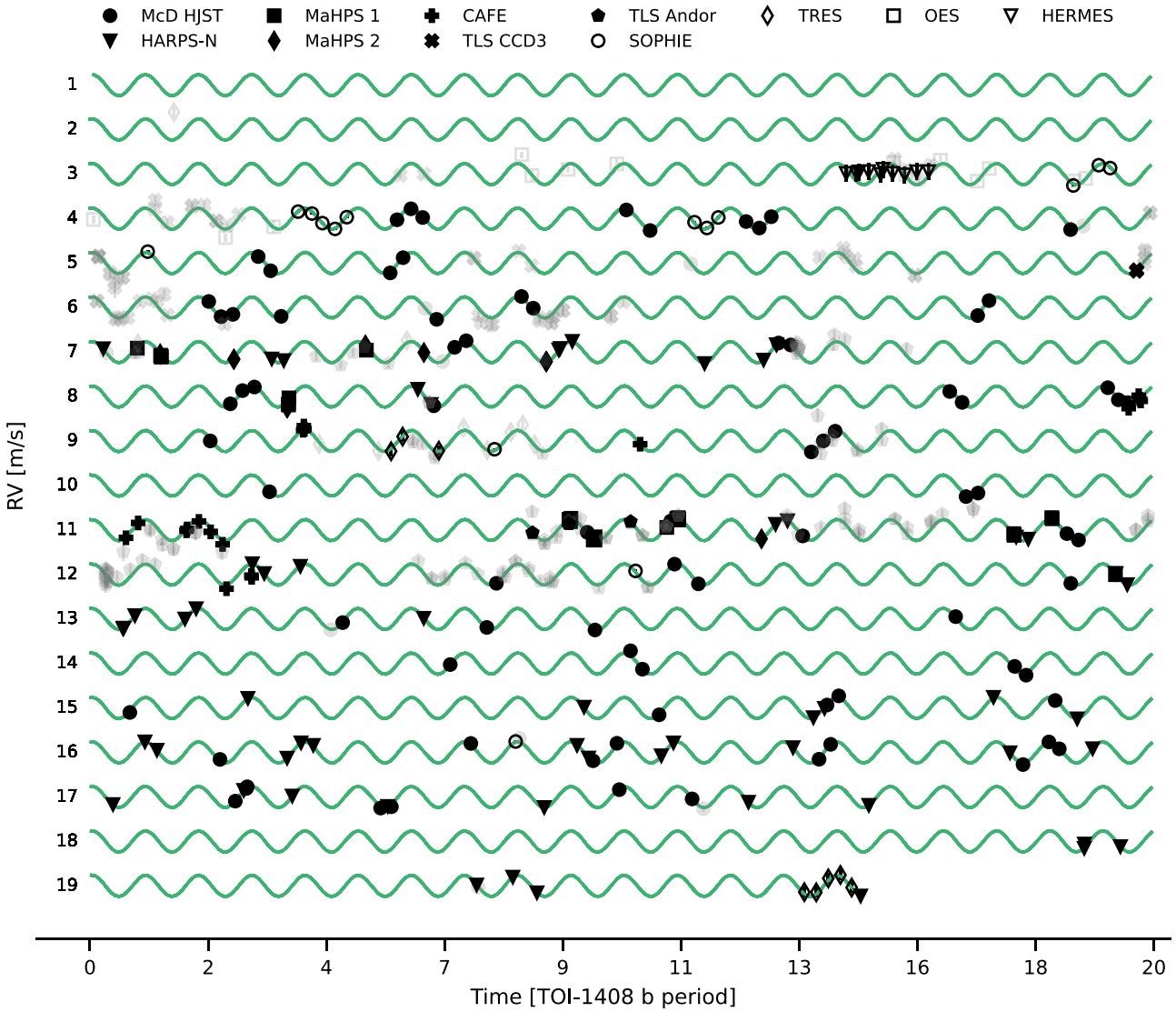


**Figure 6.** RV observations together with the model from the photodynamical analysis. One line covers 20 TOI-1408 b periods, after which the data and the model are offset down by 800 m $s^{-1}$. The vertical bar at line 1 shows the scale, spanning the RV range from −400 to 400 m $s^{-1}$. The light gray symbols mark RV observations with uncertainties larger than 25 m $s^{-1}$, and the black symbols observations with uncertainties smaller than 25 m $s^{-1}$.


## ORCID iDs

Judith Korth https://orcid.org/0000-0002-0076-6239
Priyanka Chaturvedi https://orcid.org/0000-0002-1887-1192
Hannu Parviainen https://orcid.org/0000-0001-5519-1391
Ilaria Carleo https://orcid.org/0000-0002-0810-3747
Michael Endl https://orcid.org/0000-0002-7714-6310
Eike W. Guenther https://orcid.org/0000-0002-9130-6747
Grzegorz Nowak https://orcid.org/0000-0002-7031-7754
Carina M. Persson https://orcid.org/0000-0003-1257-5146
Alexander J. Mustill https://orcid.org/0000-0002-2086-3642
Juan Cabrera https://orcid.org/0000-0001-6653-5487
William D. Cochran https://orcid.org/0000-0001-9662-3496
Jorge Lillo-Box https://orcid.org/0000-0003-3742-1987
David Hobbs https://orcid.org/0000-0002-2696-1366
Felipe Murgas https://orcid.org/0000-0001-9087-1245
Michael Greklek-McKeon https://orcid.org/0000-0002-0371-1647
Hanna Kellermann https://orcid.org/0009-0006-3527-0424
Akihiko Fukui https://orcid.org/0000-0002-4909-5763
Enric Pallé https://orcid.org/0000-0003-0987-1593
Jon M. Jenkins https://orcid.org/0000-0002-4715-9460
Joseph D. Twicken https://orcid.org/0000-0002-6778-7552
Karen A. Collins https://orcid.org/0000-0001-6588-9574
Samuel N. Quinn https://orcid.org/0000-0002-8964-8377
Ján Šubjak https://orcid.org/0000-0002-5313-9722
Paul G. Beck https://orcid.org/0000-0003-4745-2242
Davide Gandolfi https://orcid.org/0000-0001-8627-9628
Savita Mathur https://orcid.org/0000-0002-0129-0316
Hans J. Deeg https://orcid.org/0000-0003-0047-4241
David W. Latham https://orcid.org/0000-0001-9911-7388
Simon Albrecht https://orcid.org/0000-0003-1762-8235
David Barrado https://orcid.org/0000-0002-5971-9242
Hervé Bouy https://orcid.org/0000-0002-7084-487X
Rafael A. García https://orcid.org/0000-0002-8854-3776
Artie P. Hatzes https://orcid.org/0000-0002-3404-8358
Kai Ikuta https://orcid.org/0000-0002-5978-057X
Petr Kabáth https://orcid.org/0000-0002-1623-5352

Heather A. Knutson https://orcid.org/0000-0002-5375-4725
John Livingston https://orcid.org/0000-0002-4881-3620
Eder Martioli https://orcid.org/0000-0002-5084-168X
María Morales-Calderón https://orcid.org/0000-0001-9526-9499
Giuseppe Morello https://orcid.org/0000-0002-4262-5661
Norio Narita https://orcid.org/0000-0001-8511-2981
Jaume Orell-Miquel https://orcid.org/0000-0003-2066-8959
Dinil B. Palakkatharappil https://orcid.org/0000-0002-6812-4443
Seth Redfield https://orcid.org/0000-0003-3786-3486
Howard M. Relles https://orcid.org/0009-0009-5132-9520
Richard P. Schwarz https://orcid.org/0000-0001-8227-1020
Sara Seager https://orcid.org/0000-0002-6892-6948
Avi Shporer https://orcid.org/0000-0002-1836-3120
Marek Skarka https://orcid.org/0000-0002-7602-0046
Monika Stangret https://orcid.org/0000-0002-1812-8024
Luis Thomas https://orcid.org/0009-0006-1571-0306
Vincent Van Eylen https://orcid.org/0000-0001-5542-8870
Noriharu Watanabe https://orcid.org/0000-0002-7522-8195
Joshua N. Winn https://orcid.org/0000-0002-4265-047X

## References

Aceituno, J., Sánchez, S. F., Grupp, F., et al. 2013, A&A, 552, A31
Allard, F., Homeier, D., & Freytag, B. 2012, RSPTA, 370, 2765
Anderson, D. R., Collier Cameron, A., Delrez, L., et al. 2014, MNRAS, 445, 1114
Astropy Collaboration, Price-Whelan, A. M., Lim, P. L., et al. 2022, ApJ, 935, 167
Astropy Collaboration, Price-Whelan, A. M., Sipőcz, B. M., et al. 2018, AJ, 156, 123
Astropy Collaboration, Robitaille, T. P., Tollerud, J. E., et al. 2013, A&A, 558, A33
Babusiaux, C., Fabricius, C., Khanna, S., et al. 2023, A&A, 674, A32
Baranne, A., Queloz, D., Mayor, M., et al. 1996, A&AS, 119, 373
Batygin, K., Bodenheimer, P. H., & Laughlin, G. P. 2016, ApJ, 829, 114
Beck, P. G., Kambe, E., Hillen, M., et al. 2015, A&A, 573, A138
Becker, J. C., Vanderburg, A., Adams, F. C., Rappaport, S. A., & Schwengeler, H. M. 2015, ApJL, 812, L18
Bouchy, F., Hébrard, G., Udry, S., et al. 2009, A&A, 505, 853
Brown, T. M., Baliber, N., Bianco, F. B., et al. 2013, PASP, 125, 1031
Buchhave, L. A., Bakos, G. Á., Hartman, J. D., et al. 2010, ApJ, 720, 1118
Cabrera, J., Csizmadia, S., Erikson, A., Rauer, H., & Kirste, S. 2012, A&A, 548, A44
Cañas, C. I., Wang, S., Mahadevan, S., et al. 2019, ApJL, 870, L17
Castelli, F., & Kurucz, R. L. 2003, in IAU SYmp. 210, Modelling of Stellar Atmospheres, ed. N. Piskunov, W. W. Weiss, & D. F. Gray, 210 (San Francisco, CA: ASP), A20
Cincotta, P. M., & Simó, C. 2000, A&AS, 147, 205
Collins, K. A., Kielkopf, J. F., Stassun, K. G., & Hessman, F. V. 2017, AJ, 153, 77
Cosentino, R., Lovis, C., Pepe, F., et al. 2012, Proc. SPIE, 8446, 84461V
Cosentino, R., Lovis, C., Pepe, F., et al. 2014, Proc. SPIE, 9147, 91478C
Cutri, R. M., Skrutskie, M. F., van Dyk, S., et al. 2003, yCat, II/246
Dawson, R. I., & Johnson, J. A. 2018, ARA&A, 56, 175
Delisle, J. B., Laskar, J., Correia, A. C. M., & Boué, G. 2012, A&A, 546, A71
Endl, M., Kürster, M., & Els, S. 2000, A&A, 362, 585
Fűrész, G. 2008, PhD thesis, Univ. of Szeged, Hungary
Fogg, M. J., & Nelson, R. P. 2005, A&A, 441, 791
Fogg, M. J., & Nelson, R. P. 2007, A&A, 472, 1003
Foreman-Mackey, D., Hogg, D. W., Lang, D., & Goodman, J. 2013, PASP, 125, 306
Fridlund, M., Gaidos, E., Barragán, O., et al. 2017, A&A, 604, A16
Fukui, A., Narita, N., Tristram, P. J., et al. 2011, PASJ, 63, 287
Gaia Collaboration, Prusti, T., de Bruijne, J. H. J., et al. 2016, A&A, 595, A1
Gaia Collaboration, Vallenari, A., Brown, A. G. A., et al. 2023, A&A, 674, A1
Galazutdinov, G. A., Baluev, R. V., Valyavin, G., et al. 2023, MNRAS, 526, L111
García, R. A., Mathur, S., Pires, S., et al. 2014, A&A, 568, A10
Greklek-McKeon, M., Knutson, H. A., Vissapragada, S., et al. 2023, AJ, 165, 48
Grieves, N., Bouchy, F., Armstrong, D. J., et al. 2024, arXiv:2406.15986
He, Y., Wu, D.-H., & Jin, S. 2024, MNRAS, 530, 3934
Heidari, N., Boisse, I., Hara, N. C., et al. 2024, A&A, 681, A55
Hellier, C., Anderson, D. R., Collier Cameron, A., et al. 2012, MNRAS, 426, 739
Hellier, C., Anderson, D. R., Collier Cameron, A., et al. 2017, MNRAS, 465, 3693
Høg, E., Fabricius, C., Makarov, V. V., et al. 2000, A&A, 355, L27
Hord, B. J., Colón, K. D., Berger, T. A., et al. 2022, AJ, 164, 13
Hord, B. J., Colón, K. D., Kostov, V., et al. 2021, AJ, 162, 263
Huang, C., Wu, Y., & Triaud, A. H. M. J. 2016, ApJ, 825, 98
Huang, C. X., Quinn, S. N., Vanderburg, A., et al. 2020a, ApJL, 892, L7
Huang, C. X., Vanderburg, A., Pál, A., et al. 2020b, RNAAS, 4, 206
Hunter, J. D. 2007, CSE, 9, 90
Husser, T. O., Wende-von Berg, S., Dreizler, S., et al. 2013, A&A, 553, A6
Jenkins, J. M. 2002, ApJ, 575, 493
Jenkins, J. M., Chandrasekaran, H., McCauliff, S. D., et al. 2010, Proc. SPIE, 7740, 77400D
Jenkins, J. M., Tenenbaum, P., Seader, S., et al. 2020, in Kepler Data Processing Handbook: Transiting Planet Search, Kepler Science Document KSCI-19081-003, id. 9, ed. J. M. Jenkins
Jenkins, J. M., Twicken, J. D., McCauliff, S., et al. 2016, Proc. SPIE, 9913, 99133E
Jensen, E., 2013 Tapir: A web interface for transit/eclipse observability, Astrophysics Source Code Library, ascl:1306.007
Kabáth, P., Chaturvedi, P., MacQueen, P. J., et al. 2022, MNRAS, 513, 5955
Kabáth, P., Skarka, M., Sabotta, S., et al. 2020, PASP, 132, 035002
Kellermann, H. 2021, Commissioning of the high-resolution comb-calibrated spectrograph at the Wendelstein Observatory and development of calibration and fitting software packages for the hunt of exoplanets, Ludwig-Maximilians-Universität München, http://nbn-resolving.de/urn:nbn:de:bvb:19-300641
Korth, J., Gandolfi, D., Šubjak, J., et al. 2023, A&A, 675, A115
Kurucz, R. L. 1979, ApJS, 40, 1
Lillo-Box, J., Aceituno, J., Pedraz, S., et al. 2020, MNRAS, 491, 4496
Lin, D. N. C., Bodenheimer, P., & Richardson, D. C. 1996, Natur, 380, 606
Maciejewski, G., Golonka, J., Łoboda, W., et al. 2023, MNRAS, 525, L43
Mathur, S., García, R. A., Régulo, C., et al. 2010, A&A, 511, A46
Mayor, M., & Queloz, D. 1995, Natur, 378, 355
McCully, C., Turner, M., Volgenau, N., et al. 2018, LCOGT/banzai: Initial Release, v0.9.4, Zenodo, doi: 10.5281/zenodo.1257560
McCully, C., Volgenau, N. H., Harbeck, D.-R., et al. 2018, Proc. SPIE, 10707, 107070K
Mustill, A. J., Davies, M. B., & Johansen, A. 2015, ApJ, 808, 14
Narita, N., Fukui, A., Yamamuro, T., et al. 2020, Proc. SPIE, 11447, 114475K
Nascimbeni, V., Borsato, L., Zingales, T., et al. 2023, A&A, 673, A42
Nesvorný, D., Chrenko, O., & Flock, M. 2022, ApJ, 925, 38
Nesvorný, D., Kipping, D., Terrell, D., et al. 2013, ApJ, 777, 3
Nesvorný, D., & Vokrouhlický, D. 2016, ApJ, 823, 72
NExScI 2022, Exoplanet Follow-up Observing Program Web Service, IPAC, doi: 10.26134/EXOFOP5
Parviainen, H. 2015, MNRAS, 450, 3233
Parviainen, H. 2020, MNRAS, 499, 1633
Parviainen, H., & Aigrain, S. 2015, MNRAS, 453, 3821
Parviainen, H., & Korth, J. 2020, MNRAS, 499, 3356
Parviainen, H., Tingley, B., Deeg, H. J., et al. 2019, A&A, 630, A89
Perruchot, S., Kohler, D., Bouchy, F., et al. 2008, Proc. SPIE, 7014, 70140J
Persson, C. M., Fridlund, M., Barragán, O., et al. 2018, A&A, 618, A33
Piskunov, N., & Valenti, J. A. 2017, A&A, 597, A16
Poon, S. T. S., Nelson, R. P., & Coleman, G. A. L. 2021, MNRAS, 505, 2500
Pope, B. J. S., Parviainen, H., & Aigrain, S. 2016, MNRAS, 461, 3399
Price, K., Storn, R., & Lampinen, J. 2005, Differential Evolution (Berlin: Springer)
Quinn, S. N., White, R. J., Latham, D. W., et al. 2012, ApJL, 756, L33
Rasio, F. A., & Ford, E. B. 1996, Sci, 274, 954
Raskin, G., van Winckel, H., Hensberge, H., et al. 2011, A&A, 526, A69
Rein, H., & Liu, S. F. 2012, A&A, 537, A128
Rein, H., & Spiegel, D. S. 2015, MNRAS, 446, 1424
Rein, H., & Tamayo, D. 2015, MNRAS, 452, 376
Ricker, G. R., Winn, J. N., Vanderspek, R., et al. 2015, JATIS, 1, 014003
Santos, A. R. G., Breton, S. N., Mathur, S., & García, R. A. 2021, ApJS, 255, 17
Seader, S., Tenenbaum, P., Jenkins, J. M., & Burke, C. J. 2013, ApJS, 206, 25

Sha, L., Vanderburg, A. M., Huang, C. X., et al. 2023, MNRAS, 524, 1113
Smith, J. C., Stumpe, M. C., Van Cleve, J. E., et al. 2012, PASP, 124, 1000
Steffen, J. H., Ragozzine, D., Fabrycky, D. C., et al. 2012, PNAS, 109, 7982
Storn, R., & Price, K. 1997, J. Glob. Optim., 11, 341
Stumpe, M. C., Smith, J. C., Catanzarite, J. H., et al. 2014, PASP, 126, 100
Stumpe, M. C., Smith, J. C., Van Cleve, J. E., et al. 2012, PASP, 124, 985
Šubjak, J., Sharma, R., Carmichael, T. W., et al. 2020, AJ, 159, 151
Tamayo, D., Rein, H., Shi, P., & Hernandez, D. M. 2020, MNRAS, 491, 2885
Tran, Q. H., Bowler, B. P., Endl, M., et al. 2022, AJ, 163, 225
Tull, R. G., MacQueen, P. J., Sneden, C., & Lambert, D. L. 1995, PASP, 107, 251
Valenti, J. A., & Piskunov, N. 1996, A&AS, 118, 595
Van Der Walt, S. S., Colbert, S. C., & Varoquaux, G. G. 2011, CSE, 13, 22
Vines, J. I., & Jenkins, J. S. 2022, MNRAS, 513, 2719
Virtanen, P., Gommers, R., Oliphant, T. E., et al. 2020, NatMe, 17, 261
Vissapragada, S., Jontof-Hutter, D., Shporer, A., et al. 2020, AJ, 159, 108
Wang, J., Fischer, D. A., Horch, E. P., & Huang, X. 2015, ApJ, 799, 229
Wu, D.-H., & He, Y. 2023, AJ, 166, 267
Wu, D.-H., Rice, M., & Wang, S. 2023, AJ, 165, 171
Yee, S. W., Petigura, E. A., & von Braun, K. 2017, ApJ, 836, 77
Zechmeister, M., Köhler, J., & Chamarthi, S., 2021 viper: Velocity and IP EstimatoR, Astrophysics Source Code Library, ascl:2108.006
Zhu, W., Dai, F., & Masuda, K. 2018, RNAAS, 2, 160